Heteroatom Chemistry
Volume 24, Number 4, 2013

Synthesis and Photophysical Properties of Alkoxysilyl Derivatives of Dibenzoylmethanatoboron Difluoride

Yuriy N. Kononevich,[1] Ivan B. Meshkov,[1] Natalia V. Voronina,[1] Nikolay M. Surin,[1] Viacheslav A. Sazhnikov,[2] Andrei A. Safonov,[2] Alexander A. Bagaturyants,[2] Mikhail V. Alfimov,[2] and Aziz M. Muzafarov[1]

[1]*N. S. Enikolopov Institute of Synthetic Polymeric Materials, Russian Academy of Sciences, 117393 Moscow, Russian Federation*

[2]*Photochemistry Center, Russian Academy of Sciences, 119421 Moscow, Russian Federation*

Received 19 June 2012; revised 17 March 2013

ABSTRACT: *Alkoxysilyl derivatives of dibenzoylmethanatoboron difluoride ($DBMBF_2$) are synthesized by the hydrosilylation reaction of the corresponding O-allyl derivatives of $DBMBF_2$ with triethoxysilane. The photophysical properties of the synthesized O-allyl and alkoxysilyl derivatives are investigated. It is found that the absorption and fluorescence spectra of the $DBMBF_2$ derivatives essentially depend on the position of the O-allyl or O-propyl alkoxysilyl substituent. The highest fluorescence quantum yield is obtained for the para-position, whereas the substitution at the meta-position gives the largest bathochromic shift in the fluorescence spectrum. Density functional theory calculations of the structures and time-dependent density functional theory calculations of the gas-phase excitation and emission energies of alkoxysilyl derivatives are performed at the PBE0/SVP level of theory. Some spectral features of para-, ortho-, and meta-substituted derivatives can be adequately explained by the overlapping of two absorption bands.* © 2013 Wiley Periodicals, Inc. Heteroatom Chem 24:271–282, 2013; View this article online at wileyonlinelibrary.com. DOI 10.1002/hc.21091

Correspondence to: Yuriy N. Kononevich; e-mail: kononevich.yuriy@gmail.com.

Contract grant sponsor: Russian Ministry for Science and Education.
Contract grant numbers: 02.527.11.0009 and 16.523.11.3015.
Contract grant sponsor: Russian Foundation for Basic Research.
Contract grant number: 12-03-01103a.
Supporting Information is available in the online issue at wileyonlinelibrary.com.

INTRODUCTION

Recently, interest in the synthesis and study of difluoroboron β-diketonates (BF_2bdks) has increased because of useful photophysical and photochemical properties of these compounds [1–7]. BF_2bdks exhibit large extinction coefficients, large two-photon absorption cross section, intense fluorescence with high quantum yields, and high photostability. The fluorescence properties of many BF_2bdks have been studied in solution and in crystal state [8–19].

The introduction of these compounds into a polymer gives rise to new optical materials with interesting fluorescence properties [20]. In particular, polylactide modified by BF_2bdk [21–23] can be used for biological visualization, sensing, and photodynamic therapy because of high biocompatibility of polylactide polymers [24–26].

BF_2bdks in their singlet-excited state undergo photocycloaddition with alkenes and arenes; therefore, they can serve as starting compounds for the

synthesis of 1,5-diketones [27–34]. BF_2bdks are used in the design of a new polymethine dye with intense long-wavelength absorption [35, 36].

A distinctive feature of BF_2bdks is their ability to form exciplexes in the first excited singlet states with aromatic hydrocarbons that have strong fluorescence with a fluorescence maximum shifted to longer wavelengths [37–42]. The magnitude of the shift depends on the electron-donating ability of the hydrocarbon. The stronger the electron-donating properties of a hydrocarbon, the larger the shift of the fluorescence maximum to longer wavelengths.

This feature allows BF_2bdks to be used as chemical sensors for aromatic hydrocarbons [43,44]. Silica in its various forms is one of the most promising substrates for the deposition of molecular systems with sensing capabilities. It is widely used in a variety of sensing systems. The immobilization of BF_2bdks on the surface of silica particles is relevant and promising. The functionalization of BF_2bdks to form silyl-functionalized derivatives is an optimal solution to this problem.

In this article, we describe the synthesis and photophysical properties of dibenzoylmethanatoboron difluoride ($DBMBF_2$) derivatives containing a spacer with a terminal alkoxysilyl group.

RESULTS AND DISCUSSION

Synthesis

The general pathway for the synthesis of alkoxysilyl derivatives of boron difluoride β-diketonates is shown in Scheme 1. O-Allyl derivatives were obtained by the known method involving the interaction of boron trifluoride etherate with the corresponding diketones [13].

The synthesis of O-allyl derivatives of β-diketones **3a–3c** was carried out by the Claisen condensation (Scheme 1). β-Diketones **3a** and **3b** were obtained by the reaction of acetophenone **2** and methyl esters of 2- and 3-O-allyl benzoic acids **1a** and **1b**, respectively, in the presence of sodium hydride in benzene. For the synthesis of β-diketone **3c**, ethyl benzoate **4** and 4-O-allylacetophenone **5** were used. The yield of products was 68%–76%.

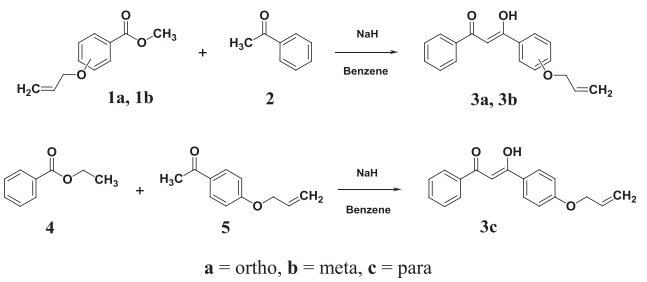

a = ortho, **b** = meta, **c** = para

SCHEME 1 Synthesis of 1,3-diaryl-propane-1,3-diones **3a–3c**.

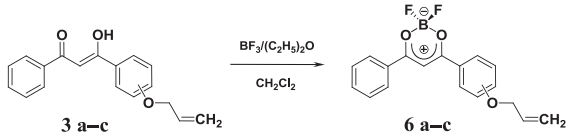

a = ortho, **b** = meta, **c** = para

SCHEME 2 Synthesis of β-diketonatoboron difluorides **6a–6c**.

Boron difluoride complexes **6a–6c** were obtained by the reaction of the corresponding β-diketones **3a–3c** with boron trifluoride diethyl etherate in dichloromethane (Scheme 2). The reaction proceeded to completion in 1 h at room temperature. After completion of the reaction, the solvent was removed in vacuo and the residue was recrystallized from toluene. A crystalline substance with an intense yellow color was formed. The product yield was 59%–64%.

The obtained boron complexes were modified to form alkoxysilyl derivatives by the hydrosilylation of O-allyl derivatives of boron difluoride β-diketonates **6a–6c** with triethoxysilane in the presence of a platinum catalyst. The reaction was carried out in tetrahydrofurane (THF) in the presence of 1,3-divinyl-1,1,3,3-tetramethyldisiloxane platinum (Scheme 3). The reaction was completed in 8 h at room temperature, as evidenced by the complete disappearance of signals of allylic protons in the ^{1}H NMR spectrum. It was found that the reduction of the double bond proceeded in parallel with hydrosilylation with a yield of 15%–25%, depending on the isomer. The formation of side products of this kind is typical for the hydrosilylation reaction [45]. The reaction products were separated by gel permeation chromatography (GPC).

To investigate the photophysical properties of the synthesized boron difluoride β-diketonate derivatives **7a–7c,** containing a spacer with the terminal alkoxysilyl group, the absorption and fluorescence spectra of corresponding model compounds **9** (Fig. 1) and **6a–6c** were measured in THF solutions and compared with the corresponding spectra of alkoxysilyl derivatives.

UV–Vis and Fluorescence Studies

Photographs of the fluorescence of synthesized compounds **6a–6c** are shown in Fig. 2.

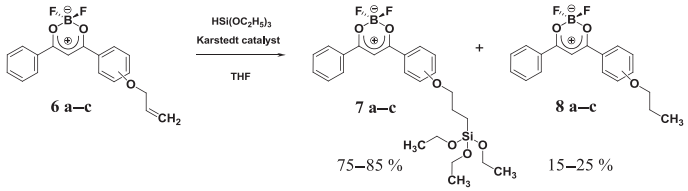

SCHEME 3 Hydrosilylation of β-diketonatoboron difluorides.

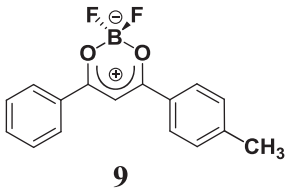

9

FIGURE 1 Model compound **9**.

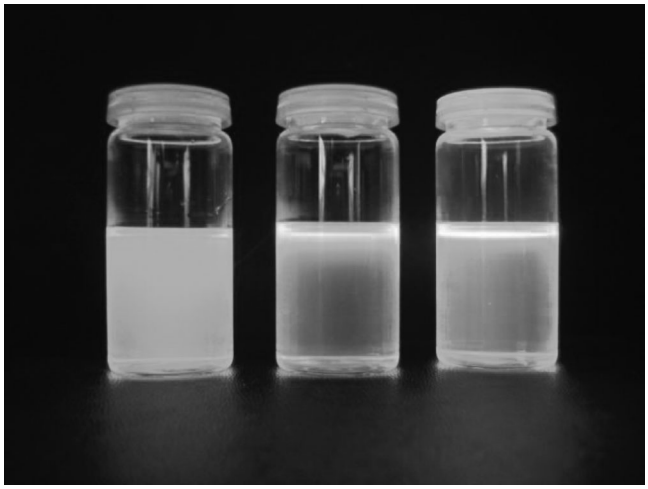

FIGURE 2 Photographs of solutions of **6a–6c** in THF excited with black light at 365 nm (from left to right: **6a**, **6b**, and **6c**, respectively).

The molar absorption coefficient was determined for solutions with a concentration of 5×10^{-5} mol/L. A solution of rhodamine 6G was used as a standard for measuring the fluorescence quantum yield ($\Phi_F = 0.94$–0.96) [46]. The energy of the purely electronic 0–0 transition was determined by the intersection of the normalized absorption and emission spectra.

The absorption and fluorescence emission spectra of the studied compounds are shown in Figs. 3–5, and spectral characteristics are given in Table 1.

As can be seen in Fig. 3, the long-wavelength absorption band of **9** consists of two resolved peaks at 386 and 370 nm and a low-intensity shoulder at about of 353 nm (25,900, 27,030 and 28,330 cm^{-1}, respectively). The second absorption region includes two peaks at 288 and 272 nm (the wavenumber separation about 2040 cm^{-1}). The fluorescence peaks of **9** are centered at 400, 420, and 445 nm (25,000, 23,810 and 22,470 cm^{-1}, respectively). Thus, the wavenumber separations between the peaks of absorption and fluorescence bands are about 1150 and 1300 cm^{-1}, which seems to correspond to a usual vibrational progression. As has been shown previously [47], the shapes of the better resolved absorption (320–400 nm) and fluorescence (400–500 nm) bands of $DBMBF_2$ in hexane can be adequately described as a superposition of vibronic bands with vibrational frequencies of 1200–1300 cm^{-1}.

The substitution of the O-allyl group for the methyl group at the para-position leads to a batochromic shift (~10 nm) of the absorption bands. The fluorescence band of **6c** is also redshifted as compared to **9** but does not reveal any visible vibronic structure.

Figure 4 shows that the absorption bands of ortho (**6a**) or meta (6b) O-allyl substituted derivatives are slightly blueshifted and broadened compared to **6c**, whereas their broad fluorescence bands are significantly redshifted. It should also be noted that **6a** exhibits a well-resolved and relatively intense peak at about 343 nm.

Figure 5 shows that the spectral properties of **7a–c** are very similar to those of **6a–6c**.

As seen in Table 1, there is a very strong dependence of the molar extinction coefficients and quantum yields on the substituent position. In particular, the para-substitution (compounds **6c** and **7c**) leads to near-unity quantum yields whereas the quantum yields of only 0.3 (comparable with that of **9**) are obtained for meta-substututed derivatives (**6b** and **7b**). Ortho-substituted **6a** exhibits a somewhat higher quantum yield (about 0.6).

Thus, the absorption and fluorescence spectra of **6a–6c** depend significantly on the position of the O-allyl substituent. Further support for this statement is the fact that the photophysical properties of β-diketonatoboron difluorides **7a–7c,** containing a spacer with a terminal alkoxysilyl group, are almost identical to the photophysical properties of **6a–6c**.

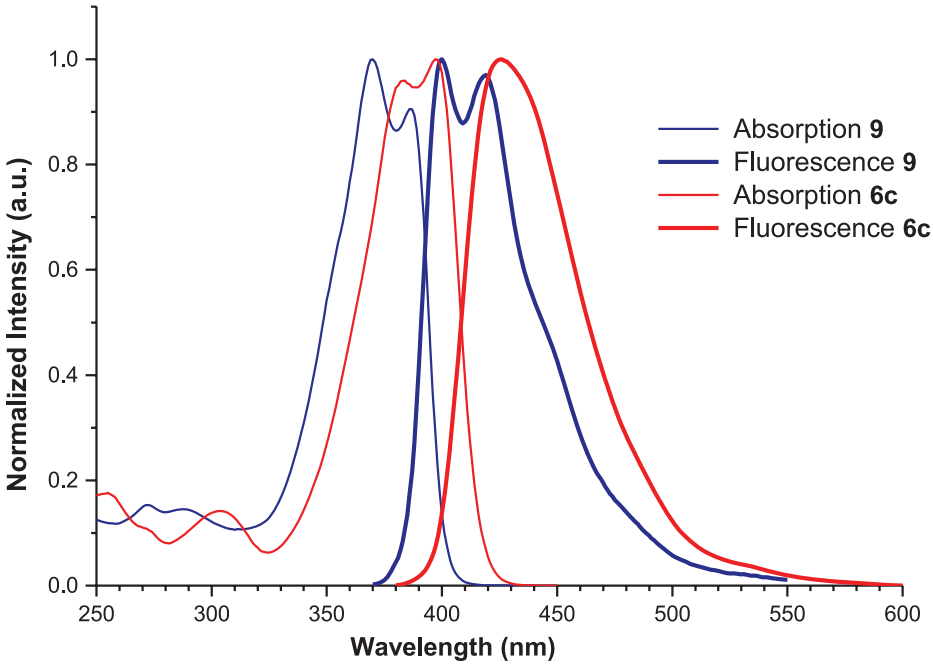

FIGURE 3 Absorption and fluorescence emission spectra of β-diketonatoboron difluorides **9** and **6c**.

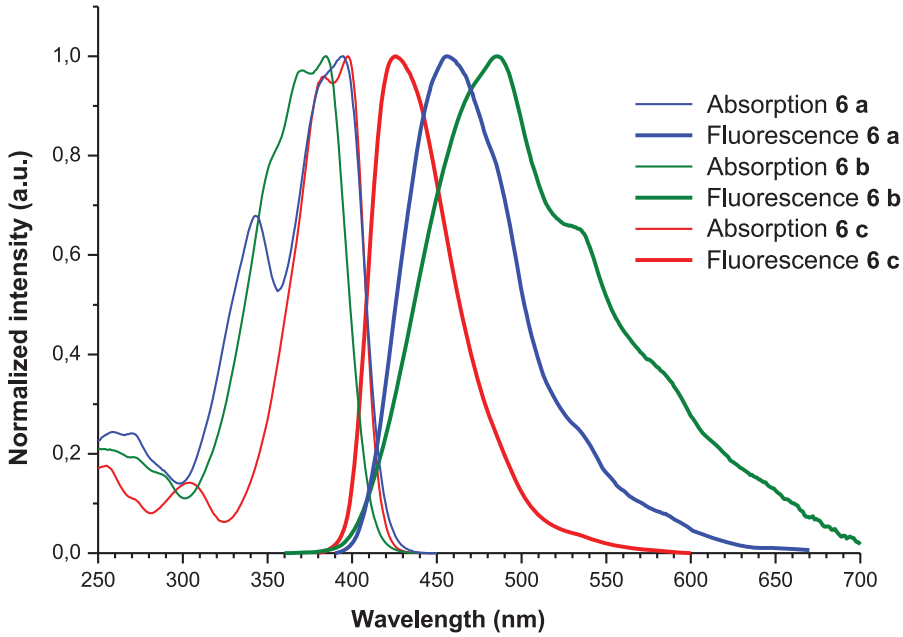

FIGURE 4 Absorption and fluorescence emission spectra of β-diketonatoboron difluorides **6a–6c**.

It can be suggested that the observed changes in photophysical properties and the difference in the calculated spectra of different isomers (compounds **6a**–**6c**) are attributable to the difference in the mesomeric and inductive effects of the oxygen atom in the ortho, meta, and para-positions. Thus, it was shown in [48] that the substitution effect of the methoxy group depends on its position in the phenyl ring: In ortho- or para-positions, it acts as a mesomeric electron donor whereas it acts as an inductive electron acceptor in meta-positions.

Density Functional Theory Results

To provide an assignment of the observed spectra, the geometrical structures and electronic absorption

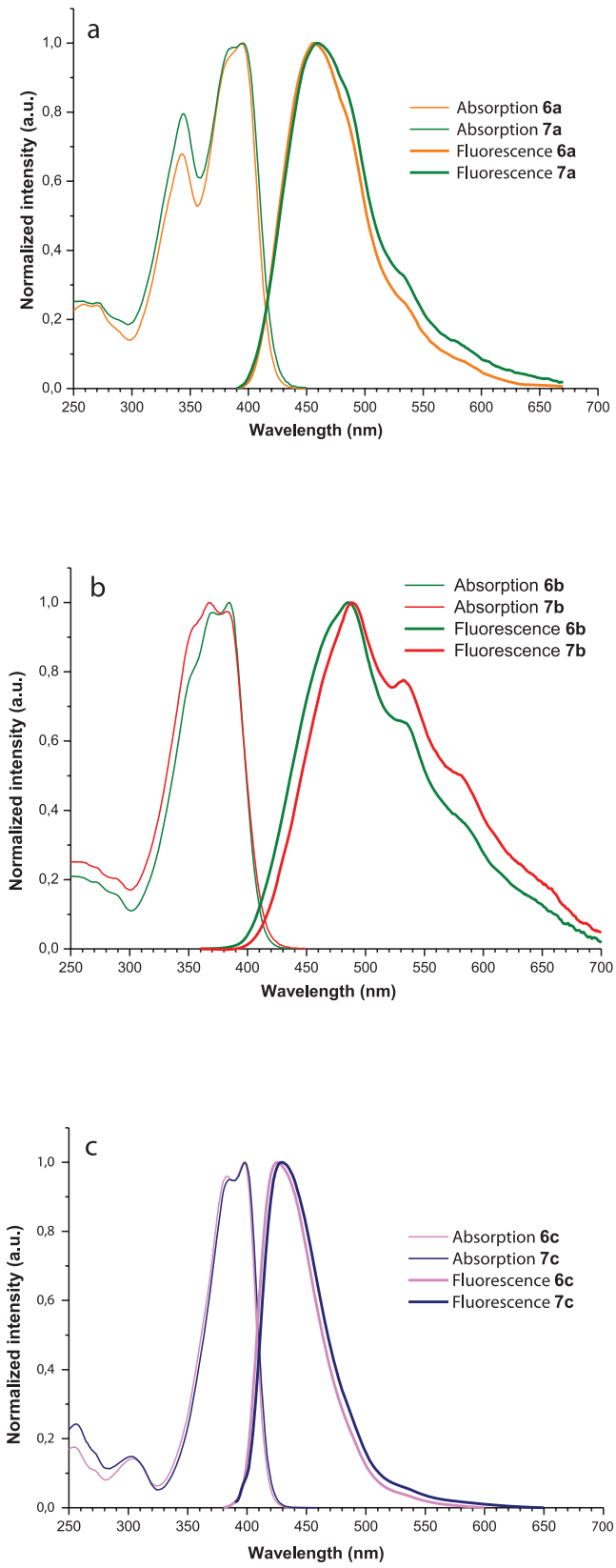

FIGURE 5 Absorption and fluorescence emission spectra of β-diketonatoboron difluorides: (a) **6a** and **7a**; (b) **6b** and **7b**; (c) **6c** and **7c**.

and fluorescence emission spectra of compounds **9** and **6a–6c** were studied theoretically by quantum-chemical density functional theory (DFT) and time-dependent density functional theory (TDDFT) calculations (details are described in the Experimental).

As an example, the calculated optimized geometries for **9** in the ground and the first excited states are shown in Fig. 6. The results for compounds **6a–6c** are given in Fig. S1 and Table S1 (in the Supporting Information).

As seen in Fig. 6, the excitation of **9** involves the following conformation changes: an increase (~7°) in the dihedral angle between BF_2 fragment and the plane of the central ring, a decrease (~6°) in the torsion angles between the phenyl rings and the central ring, a shortening of the C—C bonds connecting these rings, and some changes in the C—C bond lengths of phenyl rings.

It was found that similar changes in geometries are also characteristic of compounds **6a–6c** (Table S1 in the Supporting Information), despite of the fact that they have different equilibrium structures.

The energies of the frontier molecular orbitals for the ground and first excited states of the studied compounds are presented in Table 2. The vertical electronic transition energies for absorption and emission, oscillator strengths, main configurations, and configuration interaction (CI) coefficients of the low-lying electronically excited states are listed in Table 3.

TDDFT calculations, in agreement with the experimental data, indicate that for **9** there is only one long-wavelength absorption peak in the region of 320–400 nm. The nature of this intense band is mainly due to the electronic HOMO → LUMO transition ($f = 0.880$, CI = 0.998). The calculated transition energy 3.65 eV (339 nm) for **9** is somewhat higher than the experimental value of 3.21 eV (386 nm).

The calculated transition energy for emission is also overestimated (by 0.35 eV), but the calculated Stokes shift (1600 cm^{-1}) matches well the experimental value of 900 cm^{-1}. Table 3 shows that for **9** the calculated emission wavelength of 359 nm corresponds to experimental one at 400 nm. Thus, it is seen that conformational transformations in the S_1 state lead mainly to a considerable (by ~0.2 eV) increase in the HOMO orbital energy. It should be noted that the decrease in the HOMO—LUMO energy gap is approximately equal to the calculated difference in the vertical excitation and emission transitions.

The calculated HOMO and LUMO orbitals of **9** involved in the vertical transitions, corresponding orbital energies and wavelengths of vertical

TABLE 1 Optical Properties of **9**, **6a–6c**, and **7a–7c**

	Absorbance		*Fluorescence*		
Compound	λ_{abs} *(nm)*	ε *(M^{-1} cm^{-1})*	λ_{em} *(nm)*	Φ_F *(%)*	*0–0 Transition Energy, E_{00} (eV)*
6a	395	26,820	456	57	2.99
6b	385	32,680	485	34	3.02
6c	397	47,380	426	96	3.04
7a	396	17,710	458	29	2.97
7b	367	26,880	488	24	2.99
7c	398	42,770	429	86	3.02
9	370	43,900	400	30	3.16

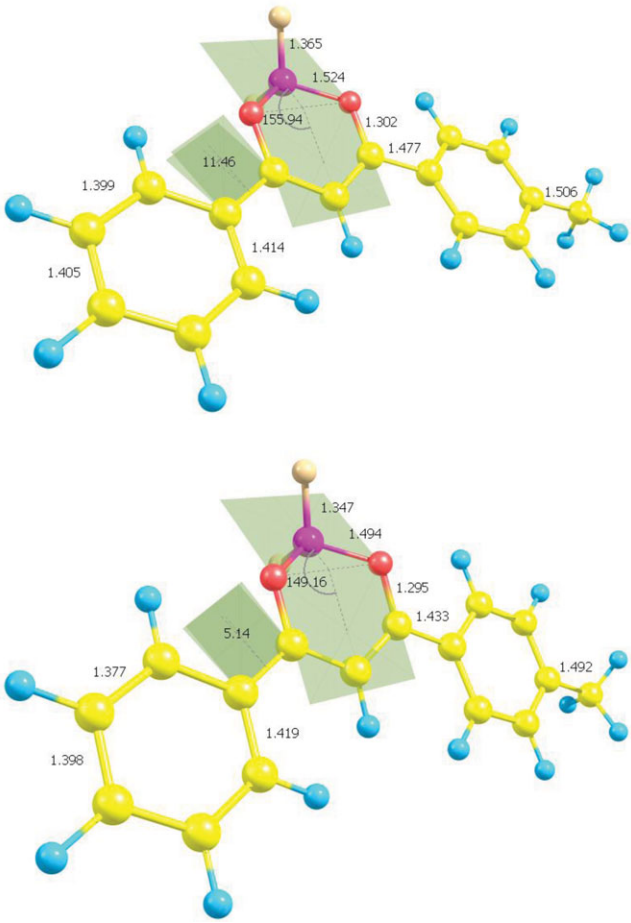

FIGURE 6 Calculated equilibrium configurations of **9** in the (top) ground and (bottom) first excited states.

transitions (Table 3) are dramatically illustrated in Fig. 7.

It should be noted that the second calculated transition for **9** at 4.18 eV (296 nm) has a small oscillator strength (0.013) and corresponds to HOMO-1 → LUMO ($S_0 \rightarrow S_2$) transition. It may be attributed to the observed weak absorption band at 288 nm. In the 300-nm region, calculations reveal a third close-lying transition (4.21 eV, $f = 0.22$), which can be related to HOMO-2 → LUMO transition.

It is well known that methoxy (or the like) groups have a stronger electron-donating ability than methyl groups. Therefore, it may be expected that the substitution of a methyl group for an alkoxy group in the para-position can result in redshifts of calculated absorption and emission bands.

The most favorable calculated structures and the corresponding HOMOs and LUMOs of isomers **6c**, **6a,** and **6b** (ground state geometry) are shown in Figs. 8–10.

Figures 8–10 show that the frontier MOs involved in the vertical transitions for absorption and emission in **6a–6c** are significantly different from those of **9**. In all the cases, the introduction of an oxygen atom leads to a significant change in the electron density distribution in the ground state and to electron density transfer from the oxygen atom to conjugated rings upon excitation. As can be seen, these effects are most pronounced for meta-substituted compound **6b**.

Table 2 shows that the oxygen lone pair affects significantly the orbital energy levels, thus changing the energy gaps. For example, the energies of HOMO and LUMO for **6c** (−6.82 and −2.72 eV, respectively) are higher than those for HOMO and LUMO of **9** (−7.10 and −2.85 eV). As a result, the calculated absorption transition is redshifted by 10 nm (Table 2), in good agreement with the experimental data (Fig. 3). In addition, this leads to an increase in the oscillator strength up to unity, which may explain the greater extinction coefficient and the higher quantum yield for **6c** (47,380 M^{-1} cm^{-1}; 0.96) as compared to **9** (43,900 M^{-1} cm^{-1}; 0.30).

Table 2 shows that ortho and meta substitutions lead to additional upward shifts of the energy levels of the HOMO and especially HOMO-1 orbitals (see Fig. S2 in the Supporting Information). This leads to a stronger interaction between the HOMO → LUMO and HOMO-1 → LUMO transitions in **6a** and **6b**. As a consequence, the second transition in **6a** is redshifted and their intensity increases in comparison with **6c** and for **6b** this transition exhibits a greater intensity as compared to the

TABLE 2 Molecular Orbital Energies (eV) of **9** and **6a–6c** in the Ground and Relaxed S_1 States Calculated at the PBE0/SVP Level of Theory.

Compound	*State*	*LUMO*	*HOMO*	*HOMO-1*	*HOMO-2*
9	S_0	–2.85	–7.10	–7.79	–7.85
	S_1	–2.88	–6.89	–7.83	–7.95
6c	S_0	–2.72	–6.82	–7.52	–7.78
	S_1	–2.73	–6.64	–7.47	–7.91
6a	S_0	–2.73	–6.88	–7.29	–7.74
	S_1	–2.74	–6.68	–7.25	–7.87
6b	S_0	–2.88	–6.80	–7.31	–7.80
	S_1	–2.96	–6.53	–7.31	–7.89

HOMO → LUMO transition. This statement is strikingly illustrated in Fig. S3 (in the Supporting Information).

It is interesting to note that these results provide a possible explanation for main features of the absorption and fluorescence of compounds **6a** and **6b**. The observed small blueshits and a broadening of their absorption bands, as well as the appearance of a peak at 343 nm in the absorption spectrum of **6a** may be a consequence of the contribution of the second HOMO-1 → LUMO transition to combined absorption in the 300–400 nm wavelength region. At the same time, the fluorescence bands of **6a** and **6b** corresponding to the LUMO → HOMO transitions exhibit redshifted wavelengths, weaker oscillator strengths and, consequently, smaller quantum yields as compared to **6c,** which correlates well with the experimental data.

An alternative explanation, of course, may involve the redistrubution of relative vibronic intensities of the first transitions due to conformation strains or solvent effects.

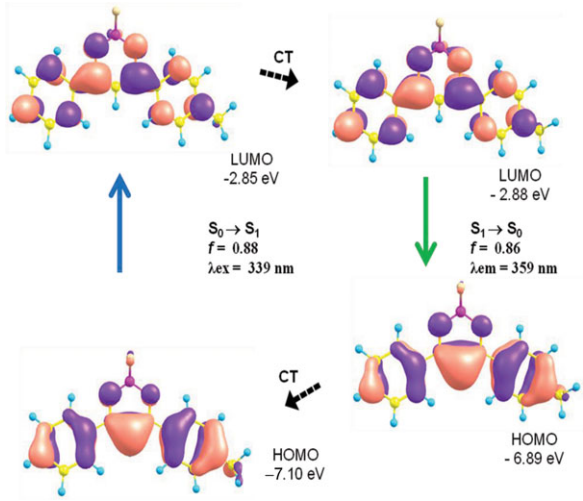

FIGURE 7 Frontier molecular orbitals involved in the vertical excitation and emission of **9**. The dotted arrows represent conformational transformations.

CONCLUSIONS

Thus alkoxysilyl derivatives of boron difluoride β-diketonates have been synthesized by the hydrosilylation reaction of the corresponding O-allyl derivatives of boron difluoride β-diketonates with triethoxysilane. The hydrosilylation reaction is accompanied by the reduction of the double bond in the O-allyl substituent with a yield of 15%–25%, depending on the O-allyl position in the phenyl

TABLE 3 Electronic Excitation and Emission Energies, Oscillator Strengths (*f*), Main Configurations, and Configuration Interaction (CI) Coefficients of the Low-Lying Electronically Excited States for **9** and **6a–6c**

Compound	*Transition*	*Energy (eV/nm)*	*f*	*Composition*	*CI*
9	$S_0 \rightarrow S_1$	3.65/339	0.880	HOMO → LUMO	0.998
	$S_0 \rightarrow S_2$	4.18/296	0.013	HOMO-1 → LUMO	0.816
				HOMO-2 → LUMO	0.184
	$S_1 \rightarrow S_0$	3.45/359	0.861		
6c	$S_0 \rightarrow S_1$	3.54/350	1.000	HOMO → LUMO	0.994
				HOMO-1 → LUMO	0.081
	$S_0 \rightarrow S_2$	4.23/293	0.035	HOMO-1 → LUMO	0.909
				HOMO → LUMO	0.065
	$S_1 \rightarrow S_0$	3.39/366	0.989		
6a	$S_0 \rightarrow S_1$	3.48/357	0.445	HOMO → LUMO	0.980
				HOMO-1 → LUMO	0.172
	$S_0 \rightarrow S_2$	3.89/319	0.295	HOMO-1 → LUMO	0.970
				HOMO → LUMO	0.181
	$S_1 \rightarrow S_0$	3.30/376	0.499		
6b	$S_0 \rightarrow S_1$	3.31/375	0.194	HOMO → LUMO	0.986
				HOMO-1 → LUMO	0.113
	$S_0 \rightarrow S_2$	3.77/329	0.660	HOMO-1 → LUMO	0.985
				HOMO → LUMO	0.125
	$S_1 \rightarrow S_0$	2.97/417	0.128		

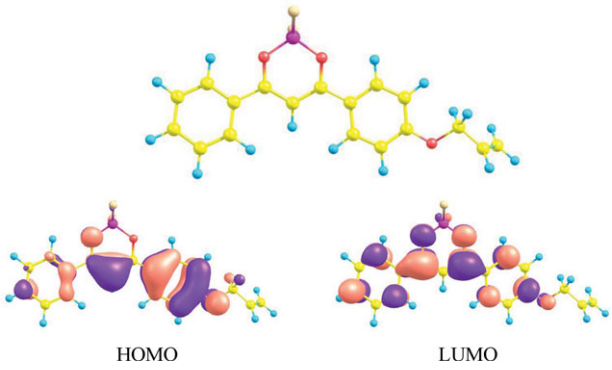

FIGURE 8 Optimized structure and molecular orbitals (HOMO and LUMO) of compound **6c**.

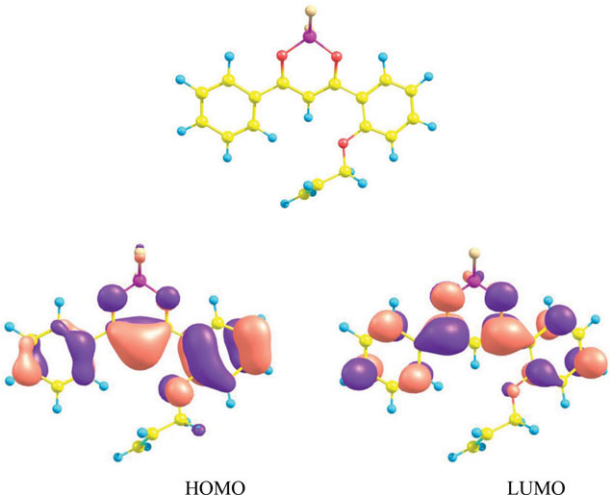

FIGURE 9 Optimized structure and molecular orbitals (HOMO and LUMO) of compound **6a**.

ring. The absorption and fluorescence spectra of boron difluoride β-diketonates essentially depend on the position of the O-allyl or O-propyl alkoxysilyl substituent. In particular, the highest fluorescence quantum yield and the greatest long-wavelength shift of the fluorescence spectrum are attained in the cases of para- and meta-positions, respectively. Theoretical calculations of the absorption and emission spectra at the TDDFT–PBE0/SVP level are in satisfactory agreement with the obtained experimental data. However, a more detailed analysis of the vibronic structure of the absorption and fluorescence bands of different derivatives would provide a better understanding of its origin. This work is currently in progress.

EXPERIMENTAL

General Methods

All solvents were purified before use. THF and benzene were distilled from sodium/benzophenone, and

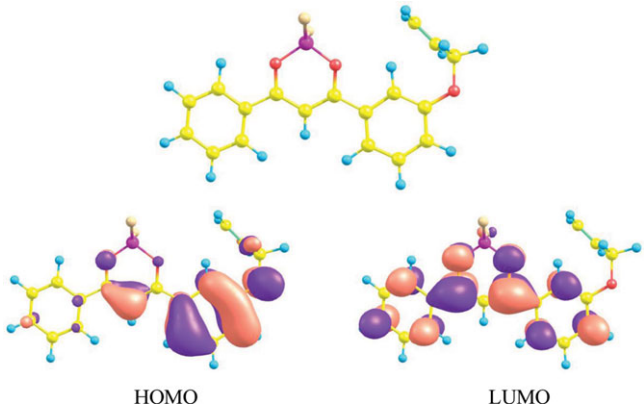

FIGURE 10 Optimized structure and molecular orbitals (HOMO and LUMO) of compound **6b**.

dichloromethane was distilled over phosphorus pentoxide. Methyl esters of 2- and 3-O-allyl benzoic acids **1a,b**, respectively, and 4-O-allylacetophenone **5** were prepared using methods described in the literature [49, 50]. All other purchased reagents were used without further purification. The reactions were monitored by thin-layer chromatography using Fluka silica gel (60 F 254) plates (0.25 mm). Column chromatography was carried out using Merck 60 (230–400 mesh) silica gel. Visualization was made with UV light. Melting points of synthesized compounds were taken on a melting point tube. Infrared spectra were recorded on Bruker Equinox 55/S spectrometer (Germany). ^{1}H NMR spectra were recorded on a Bruker WP 250 SY spectrometer (250.13 MHz; Germany). ^{13}C, ^{19}F, and ^{29}Si NMR spectra were recorded on a Bruker DRX500 spectrometer (Germany). Chemical shifts are reported relative to chloroform (δ = 7.25 ppm) or dimethyl sulfoxide (δ = 2.50 ppm) for ^{1}H NMR, chloroform (δ = 77.00 ppm) for ^{13}C NMR. High-resolution mass spectra (HRMS) were measured using a Bruker micrOTOF II instrument (Germany) with electrospray ionization (ESI). The absorption spectra were recorded on a Shimadzu UV-25001PC spectrophotometer (Japan) in THF solution. The fluorescence spectra were measured on the scanning spectrofluorimeter developed and constructed at Institute of Synthetic Polymeric Materials, Russian Academy of Sciences, Moscow, Russian Federation, equipped with a 150-W arc xenon lamp as the pumping source, two Seya-Namioka-type monochromators and two photoelectronic multipliers [51].

Computational Details

Geometry optimization for the ground electronic state was performed by DFT with the Perdew-Burke-Ernzerhof (PBE) functional and Ahlrichs'

double-zeta polarized Split Valence Polarization (SVP) basis set using the ORCA program [52]. Structures in the excited electronic state, which are responsible for the fluorescence spectra, were optimized using the time-dependent DFT (TDDFT) method with the Becke-Half-and-Half-Lee-Yang-Parr (BH and HLYP) functional and the SVP basis set.

At the optimized geometries, the absorption and fluorescence spectra were calculated using the TDDFT method with the PBE0 functional and the SVP basis set. TDDFT calculations were performed using the Firefly program [53], which is partially based on the GAMESS (US) [54] source code.

*General Procedure for the Synthesis of 1,3-Diaryl-propane-1,3-diones (**3a–3c**)*

The solution of ketone (0.05 mol) and ester (0.05 mol) in dry benzene (30 mL) was added to suspension of sodium hydride (1.32 g, 0.055 mol) in dry benzene (20 mL) under inert atmosphere. The resulting mixture was heated at reflux for 8 h. Suspension was cooled to room temperature and poured into dilute HCl (5%, 100 mL). An organic layer was isolated with a separating funnel and washed with aqueous Na_2CO_3, then H_2O. After drying over Na_2SO_4, the solvent was evaporated in vacuo. The residual product was purified by recrystallization from isopropanol.

1-Phenyl-3-[2-(prop-2-en-1-yl-oxy)phenyl]propane-1,3-dione, **3a**. Yield: 68%, mp 55–57°C. ^{1}H NMR (300 MHz, $CDCl_3$): δ 4.67 (d, 2H, J = 5.3 Hz, O—CH_2), 5.33–5.54 (m, 2H, C=CH_2), 6.08–6.20 (m, 1H, CH=C), 6.98 (d, 1H, J = 8.2 Hz, Ar), 7.07 (t, 1H, J = 7.3 Hz, Ar), 7.27 (s, 1H, CO—CH—CO), 7.42–7.56 (m, 4H, Ar), 7.94–7.99 (m, 3H, Ar). ^{13}C NMR (75 MHz, $CDCl_3$): δ 69.4, 98.6, 112.9, 118.3, 121.0, 125.0, 127.2, 128.4, 128.5, 128.6, 130.3, 132.2, 132.6, 133.0, 135.9, 157.5, 183.8, 185.6. IR (CsI): 3082, 1606, 1564, 1275, 1244, 1009, 937, 760 cm^{-1}. UV–vis (THF) λ = 356 nm (ε = 22,960 L/mol*cm). HRMS (ESI) *m/z* calcd. for $C_{18}H_{16}NaO_3$ [$(M + Na)^+$]: 303.0992, found 303.0989. Elemental analysis calcd. for $C_{18}H_{16}O_3$: C, 77.12; H, 5.75. Found: C, 77.29; H, 5.75.

1-Phenyl-3-[3-(prop-2-en-1-yl-oxy)phenyl]propane-1,3-dione, **3b**. Yield: 72%, mp 40–42°C. ^{1}H NMR (300 MHz, $CDCl_3$): δ 4.61 (d, 2H, J = 4.9 Hz, O—CH_2), 5.30–5.48 (m, 2H, C=CH_2), 6.00–6.16 (m, 1H, CH=C), 6.83 (s, 1H, CO—CH—CO), 7.09–7.13 (m, 1H, Ar), 7.38 (t, 1H, J = 7.9 Hz, Ar), 7.45–7.57 (m, 5H, Ar), 7.98 (d, 2H, J = 6.7 Hz, Ar), 11.49 (s, 1H, OH). ^{13}C NMR (75 MHz, $CDCl_3$): δ 68.9, 93.3, 112.9, 118.0, 119.2, 119.7, 127.1, 128.7, 129.6, 132.4, 132.8, 135.4, 137.0, 158.8, 185.4, 185.7. IR (CsI): 3076, 2981, 2845, 1604, 1576, 1489, 1257, 1203, 1028, 920, 764, 683 cm^{-1}. UV–vis (THF) λ = 357 nm (ε = 26,000 L/mol*cm). HRMS (ESI) *m/z* calcd. for $C_{18}H_{16}NaO_3$ [$(M + Na)^+$]: 303.0992, found 303.0988. Elemental analysis calcd. for $C_{18}H_{16}O_3$: C, 77.12; H, 5.75. Found: C, 77.16; H, 5.77.

1-Phenyl-3-[4-(prop-2-en-1-yloxy)phenyl]propane-1,3-dione, **3c**. Yield: 76%, mp 48–50°C. ^{1}H NMR (300 MHz, DMSO-d_6): δ 4.69 (d, 2H, J = 4.9 Hz, O—CH_2), 5.27–5.46 (m, 2H, C=CH_2), 5.98–6.14 (m, 1H, CH=C), 7.10 (d, 2H, J = 8.6 Hz, Ar), 7.29 (s, 1H, CO—CH—CO), 7.52–7.66 (m, 3H, Ar), 8.14–8.18 (m, 4H, Ar), 15.10 (s, 1H, OH). ^{13}C NMR (75 MHz, $CDCl_3$): δ 68.9, 92.3, 114.6, 118.2, 127.0, 128.2, 128.6, 129.3, 132.1, 132.5, 135.5, 162.2, 184.0, 186.1. IR (CsI): 3078, 2929, 1605, 1510, 1259, 1176, 1014, 922, 841, 766 cm^{-1}. UV–vis (THF) λ = 353 nm (ε = 23,180 L/mol*cm). HRMS (ESI) *m/z* calcd. for $C_{18}H_{16}NaO_3$ [$(M + Na)^+$]: 303.0992, found 303.0992. Elemental analysis calcd for $C_{18}H_{16}O_3$: C, 77.12; H, 5.75. Found: C, 77.15; H, 5.78.

*General Procedure for the Synthesis of β-Diketonatoboron difluorides (**6a–6c**)*

To a solution of 1,3-diaryl-propane-1,3-dione (0.01 mol) in dry dichloromethane (30 mL), boron trifluoride-diethyl etherate (0.012 mol) was added. The reaction mixture was stirred for 1 h at room temperature. After removing the solvent by evaporation in vacuo, the residue was purified by recrystallization from toluene.

2,2-Difluoro-4-phenyl-6-[2-(prop-2-en-1-yloxy) phenyl]-1,3,2-(2H)-dioxaborine, **6a**. Yield: 59%, mp 219–221°C. ^{1}H NMR (300 MHz, DMSO-d_6): δ 4.84 (d, 2H, J = 5.5 Hz, O—CH_2), 5.36–5.56 (m, 2H, C=CH_2), 6.13–6.29 (m, 1H, CH=C), 7.20 (t, 1H, J = 7.3 Hz, Ar), 7.34 (d, 1H, J = 8.6 Hz, Ar), 7.64–7.85 (m, 4H, Ar), 7.91 (s, 1H, CO—CH—CO), 8.03 (d, 1H, J = 7.9 Hz, Ar), 8.14 (d, 2H, J = 7.3 Hz, Ar). ^{13}C NMR (75 MHz, $CDCl_3$): δ 69.8, 98.8, 113.0, 119.6, 121.1, 121.4, 128.9, 129.0, 131.9, 132.0, 132.4, 134.9, 136.4, 159.8, 180.9, 182.6. ^{19}F NMR (282 MHz, $CDCl_3$): δ –139.59 (24%, ^{10}B–F), –139.66 (76%, ^{11}B–F). IR (CsI): 1603, 1547, 1489, 1367, 1225, 1097, 1041 cm^{-1}. UV–vis (THF) λ = 394 nm (ε = 26,860 L/mol*cm). HRMS (ESI) *m/z* calcd. for $C_{18}H_{15}BF_2NaO_3$ [$(M + Na)^+$]: 351.0978, found 351.0973. Elemental analysis calcd for $C_{18}H_{15}BF_2O_3$: C, 65.89; H, 4.61; B, 3.29; F, 11.58. Found: C, 66.01; H, 4.65; B, 3.28; F, 11.57.

2,2-Difluoro-4-phenyl-6-[3-(prop-2-en-1-yloxy) phenyl]-1,3,2-(2H)-dioxaborine, **6b**. Yield: 64%, mp 127–129°C. ^{1}H NMR (300 MHz, DMSO-d_6): δ 4.72 (d, 2H, J = 5.5 Hz, O—CH_2), 5.28–5.48 (m, 2H, C=CH_2), 6.01–6.16 (m, 1H, CH=C), 7.40–7.44 (m, 2H, Ar), 7.56–7.71 (m, 3H, Ar), 7.81–7.90 (m, 2H, Ar), 7.96–7.99 (m, 2H, Ar, CO—CH—CO), 8.40 (d, 2H, J = 7.3 Hz, Ar). ^{13}C NMR (75 MHz, $CDCl_3$): δ 68.7, 94.7, 114.7, 117.8, 121.9, 122.4, 129.4 (d, J = 2.8 Hz), 130.6, 131.2, 132.7, 133.2, 135.9, 158.7, 182.4, 182.8. ^{19}F NMR (282 MHz, $CDCl_3$): δ –136.86 (21%, ^{10}B–F), –136.92 (79%, ^{11}B–F). IR (CsI): 1541, 1485, 1379, 1363, 1263, 1047, 773 cm^{-1}. UV–vis (THF) λ = 384 nm (ε = 32,660 L/mol*cm). HRMS (ESI) *m/z* calcd. for $C_{18}H_{15}BF_2NaO_3$ [(M + Na)$^+$]: 351.0978, found 351.0967. Elemental analysis calcd for $C_{18}H_{15}BF_2O_3$: C, 65.89; H, 4.61; B, 3.29; F, 11.58. Found: C, 65.84; H, 4.61; B, 3.34; F, 11.51.

2,2-Difluoro-4-phenyl-6-[4-(prop-2-en-1-yloxy) phenyl]-1,3,2-(2H)-dioxaborine, **6c**. Yield: 61%, mp 203–205°C. ^{1}H NMR (300 MHz, DMSO-d_6): δ 4.77 (d, 2H, J = 5.5 Hz, O—CH_2), 5.30–5.47 (m, 2H, C=CH_2), 6.0–6.15 (m, 1H, CH=C), 7.22 (d, 2H, J = 9.2 Hz, Ar), 7.65 (t, 2H, J = 7.9 Hz, Ar), 7.80 (t, 1H, J = 7.3 Hz, Ar), 7.86 (s, 1H, CO=CH=CO), 8.33–8.42 (m, 4H, Ar). ^{13}C NMR (75 MHz, $CDCl_3$): δ 69.2, 92.5, 115.3, 118.7, 124.2, 128.6, 129.0, 131.6, 131.9, 132.2, 134.7, 164.7, 181.4, 182.2. ^{19}F NMR (282 MHz, $CDCl_3$): δ –140.18 (19%, ^{10}B–F), –140.24 (81%, ^{11}B–F). IR (CsI): 1595, 1541, 1491, 1365, 1317, 1244, 1190, 1043, 999, 775, 559 cm^{-1}. UV–vis (THF) λ = 398 nm (ε = 46,600 L/mol*cm). HRMS (ESI) *m/z* calcd. for $C_{18}H_{15}BF_2NaO_3$ [(M + Na)$^+$]: 351.0978, found 351.0963. Elemental analysis calcd for $C_{18}H_{15}BF_2O_3$: C, 65.89; H, 4.61; B, 3.29; F, 11.58. Found: C, 65.75; H, 4.57; B, 3.24; F, 11.63.

General Procedure of the Hydrosilylation of β-diketonatoboron Difluorides

To a suspension of β-diketonatoboron difluoride (0.003 mol) and triethoxysilane (0.0032 mol) in dry THF (30 mL) under argone, 30 μL of a Pt catalyst was added. The reaction mixture was stirred for 8 h at room temperature. After GPC (eluent THF), the product was obtained as a yellow oil.

2,2-Difluoro-4-phenyl-6-[2-(3-(triethoxysilyl) propoxy)phenyl]-1,3,2-(2H)-dioxaborine, **7a**. Yield: 82%. ^{1}H NMR (300 MHz, $CDCl_3$): δ 0.80 (m, 2H, CH_2Si), 1.18 (t, 9H, J = 6.7 Hz, Si—O—C—CH_3), 2.08 (m, 2H, O—C—CH_2—C), 3.77 (q, 6H, J = 6.7 Hz, Si—O—CH_2—), 4.17 (t, 2H, J = 6.7 Hz, Ar—O—CH_2—), 7.01–7.12 (m, 2H, Ar), 7.51–7.69 (m, 4H, Ar), 7.85 (s, 1H, CO—CH—CO), 8.09 (d, 2H, J = 7.0 Hz, Ar), 8.22 (d, 1H, J = 8.2 Hz,). ^{13}C NMR (75 MHz, $CDCl_3$): δ 6.9, 18.3, 23.1, 58.5, 71.21, 98.7, 112.9, 121.1, 128.8, 129.1, 132.0, 134.6, 136.4, 160.5, 181.3, 182.7. ^{19}F NMR (282 MHz, $CDCl_3$): δ –140.94 (22%, ^{10}B–F), –141.01 (78%, ^{11}B–F). ^{29}Si NMR (59 MHz, $CDCl_3$): δ –46.45. IR (CsI): 2927, 1601, 1535, 1491, 1375, 1198, 1165, 1101, 1078, 1045, 958 cm^{-1}. UV–vis (THF) λ = 396 nm (ε = 17,660 L/mol*cm). HRMS (ESI) *m/z* calcd. for $C_{24}H_{31}BF_2NaO_6Si$ [(M + Na)$^+$]: 515.1848, found 515.1844. Elemental analysis calcd for $C_{24}H_{31}BF_2O_6Si$: C, 58.54; H, 6.35; B, 2.20; F, 7.72; Si, 5.70. Found: C, 56.33; H, 5.46; B, 1.75; F, 6.59; Si, 6.02.

2,2-Difluoro-4-phenyl-6-[3-(3-(triethoxysilyl) propoxy)phenyl]-1,3,2-(2H)-dioxaborine, **7b**. Yield: 75%. ^{1}H NMR (300 MHz, DMSO-d_6): δ 0.79 (m, 2H, CH_2Si), 1.23 (t, 9H, J = 6.7 Hz, Si—O—C—CH_3), 1.94 (m, 2H, O—C—CH_2—C), 3.85 (q, 6H, J = 7.3 Hz, Si—O—CH_2—), 4.03 (t, 2H, J = 6.7 Hz, Ar—O—CH_2—), 7.17 (s, 1H, CO—CH—CO), 7.21 (dd, 1H, J_1 = 2.4 Hz, J_2 = 8.5 Hz, Ar), 7.43 (t, 1H, J = 7.9 Hz, Ar), 7.55 (t, 2H, J = 7.9 Hz, Ar), 7.63–7.72 (m, 3H, Ar), 8.15 (d, 2H, J = 7.3 Hz, Ar). ^{13}C NMR (75 MHz, $CDCl_3$): δ 6.5, 18.3, 22.7, 58.5, 70.3, 93.6, 114.0, 121.2, 122.1, 128.9, 129.2, 130.1, 132.0, 133.3, 135.2, 159.7, 183.2, 183.3. ^{19}F NMR (282 MHz, $CDCl_3$): δ –140.68 (22%, ^{10}B–F), –140.74 (78%, ^{11}B–F). ^{29}Si NMR (59 MHz, $CDCl_3$): δ –45.60. IR (CsI): 2929, 1599, 1545, 1487, 1377, 1263, 1167, 1101, 1078, 1045, 960 cm^{-1}. UV–vis (THF) λ = 367 nm (ε = 26,840 L/mol*cm). HRMS (ESI) *m/z* calcd. for $C_{24}H_{31}BF_2NaO_6Si$ [(M + Na)$^+$]: 515.1848, found 515.1875. Elemental analysis calcd for $C_{24}H_{31}BF_2O_6Si$: C, 58.54; H, 6.35; B, 2.20; F, 7.72; Si, 5.70. Found: C, 55.53; H, 5.22; B, 1.80; F, 6.52; Si, 6.93.

2,2-Difluoro-4-phenyl-6-[4-(3-(triethoxysilyl) propoxy)phenyl]-1,3,2-(2H)-dioxaborine, **7c**. Yield: 85%. ^{1}H NMR (300 MHz, DMSO-d_6): δ 0.77 (m, 2H, CH_2Si), 1.23 (t, 9H, J = 7.0 Hz, Si—O—C—CH_3), 1.94 (m, 2H, O—C—CH_2—C), 3.84 (q, 6H, J = 6.9 Hz, Si—O—CH_2—), 4.06 (t, 2H, J = 6.4 Hz, Ar—OCH_2—), 6.99 (d, 2H, J = 9.2 Hz, Ar), 7.08 (s, 1H, CO—CH—CO), 7.51 (t, 2H, J = 7.3 Hz, Ar), 7.64 (t, 1H, J = 7.3 Hz, Ar), 8.10 (m, 4H, Ar). ^{13}C NMR (75 MHz, $CDCl_3$): δ 6.5, 18.3, 22.6, 58.5, 70.4, 92.4, 115.1, 116.3, 123.8, 128.6, 129.0, 131.7, 131.9, 132.3, 134.6, 165.4, 181.2, 182.2. ^{19}F NMR (282 MHz, $CDCl_3$): δ –141.64 (21%, ^{10}B–F), –141.70 (79%, ^{11}B–F). ^{29}Si NMR (59 MHz, $CDCl_3$): δ –45.97. IR (CsI): 2927, 1599, 1543, 1493, 1373, 1269,

1238, 1176, 1103, 1078, 1047, 958 cm^{-1}. UV–vis (THF) $\lambda = 398$ nm ($\varepsilon = 42{,}760$ L/mol*cm). HRMS (ESI) *m/z* calcd. for $C_{24}H_{31}BF_2NaO_6Si$ $[(M + Na)^+]$: 515.1848, found 515.1825. Elemental analysis calcd for $C_{24}H_{31}BF_2O_6Si$: C, 58.54; H, 6.35; B, 2.20; F, 7.72; Si, 5.70. Found: C, 56.98; H, 6.08; B, 1.82; F, 6.69; Si, 6.11.

REFERENCES

[1] Fabian, J.; Hartmann, H. J. Phys Org Chem 2004, 17, 359–369.
[2] Cognÿ-Laage, E.; Allemand, J.-F.; Ruel, O.; Baudin, J.-B.; Croquette, V.; Blanchard-Desce, M.; Jullien, L. Chem Eur J 2004, 10, 1445–1455.
[3] Ono, K.; Yoshikawa, K.; Tsuji, Y.; Yamaguchi, H.; Uozumi, R.; Tomura, M.; Taga, K.; Saito, K. Tetrahedron 2007, 63, 9354–9358.
[4] Guerro, M.; Roisnel, T.; Lorcy, D. Tetrahedron 2009, 65, 6123–6127.
[5] Rohde, D.; Yan, C.-J.; Wan, L.-J. Langmuir 2006, 22, 4750–4757.
[6] Görlitz, G.; Hartmann, H. Heteroatom Chem 1997, 8, 147–155.
[7] Toporcer, L. H.; Dessy, R. E.; Green, S. I. E. Inorg Chem 1965, 4, 1649–1655.
[8] Mirochnik, A. G.; Gukhman, E. V.; Karasev, V. E.; Zhikhareva, P. A. Russ Chem Bull 2000, 49, 1024–1027.
[9] Brown, N. M. D.; Bladon, P. J Chem Soc (A) 1969, 526–532.
[10] Mirochni k, A. G.; Bukvetskii, B. V.; Gukhman, E. V.; Zhikhareva, P. A.; Karasev, V. E. Russ Chem Bull 2001, 50, 1612–1615.
[11] Mirochnik, A. G.; Bukvetskii, B. V.; Gukhman, E. V.; Zhikhareva, P. A.; Karasev, V. E. Russ Chem Bull 2002, 51, 1715–1719.
[12] Mirochnik, A. G.; Bukvetskii, B. V.; Fedorenko, E. V.; Karasev, V. E. Russ Chem Bull 2004, 53, 291–296.
[13] Mirochnik, A. G.; Fedorenko, E. V.; Karpenko, A. A.; Gizzatulina, D. A.; Karasev, V. E. Luminescence 2007, 22, 195–198.
[14] Mirochnik, A. G.; Fedorenko, E. V.; Kaidalova, T. A.; Merkulov, E. B.; Kuryavyi, V. G.; Galkin, K. N.; Karasev, V. E. J. Luminescence 2008, 128, 1799–1802.
[15] Bukvetskii, B. V.; Fedorenko, E. V.; Mirochnik, A. G.; Karasev, V. E. J Struct Chem 2007, 48, 1148–1151.
[16] Ilge, H.-D.; Birckner, E.; Fassler, D.; Kozmenko, M. V.; Kuz'min, M. G.; Hartmann, H. J. Photochem 1986, 32, 177–189.
[17] Mirochnik, A. G.; Fedorenko, E. V.; Kuryavyi, V. G.; Bukvetskii, B. V.; Karasev, V. E. J Fluoresc 2006, 16, 279–286.
[18] Zhang, G.; Lu, J.; Sabat, M.; Fraser, C. L. J Am Chem Soc 2010, 132, 2160–2162.
[19] Chow, Y. L.; Johansson, C. I.; Zhang, Y.-H.; Gautron, R.; Yang, L.; Rassat, A.; Yang, S.-Z. J Phys Org Chem 1996, 9, 7–16.
[20] Zhang, G.; Clair, T. L. S.; Fraser, C. L. Macromolecules 2009, 42, 3092–3097.
[21] Zhang, G.; Fiore, G. L.; Clair, T. L. S.; Fraser, C. L. Macromolecules 2009, 42, 3162–3169.
[22] Zhang, G.; Evans, R. E.; Campbell, K. A.; Fraser, C. L. Macromolecules 2009, 42, 8627–8633.
[23] Zhang, G.; Chen, J.; Payne, S. J.; Kooi, S. E.; Demas, J. N.; Fraser, C. L. J Am Chem Soc 2007, 129, 8942–8943.
[24] Pfister, A.; Zhang, G.; Zareno, J.; Horwitz, A. F.; Fraser, C. L. ACS Nano 2008, 2, 1252–1258.
[25] Contreras, J.; Xie, J.; Chen, Y. J.; Pei, H.; Zhang, G.; Fraser, C. L.; Hamm-Alvarez, S. F. ACS Nano 2010, 4, 2735–2747.
[26] Fraser, C. L.; Zhang, G. Mater Today 2009, 12, 38–40.
[27] Chow, Y. L.; Cheng, X. J Chem Soc, Chem Commun 1990, 1043–1045.
[28] Chow, Y. L.; Ouyang, X. Can J Chem 1991, 69, 423–431.
[29] Chow, Y. L.; Cheng, X. Can J Chem 1991, 69, 1331–1336.
[30] Chow, Y. L.; Cheng, X. Can J Chem 1991, 69, 1575–1583.
[31] Chow, Y. L.; Wang, S.-S.; Cheng, X.-E. Can J Chem 1993, 71, 846–654.
[32] Chow, Y. L.; Wang, S.-S. Tetrahedron Lett 1994, 35, 9661–9664.
[33] Chow, Y. L.; Wang, S.-S.; Johansson, C. I.; Liu, Z.-L. J Am Chem Soc 1996, 118, 11725–11732.
[34] Chow, Y. L.; Cheng, X.-E.; Wang, S.-S.; Wu, S. P. Can J Chem 1997, 75, 720–726.
[35] Halik, M.; Hartmann, H. Chem Eur J 1999, 5, 2511–2517.
[36] Gerasov, A. O.; Shandura, M. P.; Kovtun, Y. P.; Vlasenko, Y. G.; Gorchev, V. F. J Heterocyclic Chem 2008, 45, 1665–1672.
[37] Valat, P.; Wintgens, V.; Chow, Y. L.; Kossanyi, J. Can J Chem 1995, 73, 1902–1913.
[38] Chow, Y. L.; Johansson, C. I. J Phys Chem 1995, 99, 17558–17565.
[39] Chow, Y. L.; Johansson, C. I. J Phys Chem 1995, 99, 17566–17572.
[40] Chow, Y. L.; Johansson, C. I.; Liu, Z.-L. J Phys Chem 1996, 100, 13381–13385.
[41] Chow, Y. L.; Liu, Z.-L.; Johansson, C. I.; Ishiyama, J. Chem Eur J 2000, 6, 2942–2947.
[42] Truong, T.-T.; Brenner, V.; Ledoux, G.; Tran-Thi, T.-H. Photochem Photobiol Sci 2006, 5, 686–697.
[43] Sazhnikov, V. A.; Aristarkhov, V. M.; Mirochnik, A. G.; Fedorenko, E. V.; Alfimov, M. V. Dokl Akad Nauk 2011, 437, 201–204.
[44] Sazhnikov, V. A.; Muzafarov, A. M.; Kopysov, V. N.; Aristarkhov, V. M.; Kononevich, Yu. N.; Meshkov, I. B.; Voronina, N. V.; Alfimov, M. V. Nanotechnol Russ 2012, 7, 6–14.
[45] Marciniec, B.; Maciejewski, H.; Pietraszuk, C.; Pawluc, P. In Hydrosilylation: A Comprehensive Review on Recent Advances; Marciniec, B., Ed.; Springer: Berlin, Germany, 2009; p. 7.
[46] Demas, J. N.; Crosby, G. A. J Phys Chem 1971, 75, 991–1024.
[47] Sazhnikov, A. M.; Kopysov, V. N.; Aristarkhov, V. M.; Shibneva, E. S.; Mirochnik, A. G.; Fedorenko, E. V.; Alfimov, M. V. High Energy Chem 2011, 45, 501–504.
[48] Bouzakraoui, S.; Bouzzine, S. M.; Bouachrinea, M.; Hamidi, M.; Solar Energy Materials & Solar Cells 2006, 90, 1393–1402.
[49] Smith, K.; Morris, I. K.; Owen, P. G.; Bass, R. J. J Chem Soc, Perkin Trans 1988, 1, 77–83.

[50] Mereyala, H. B.; Gurrala, R.; Mohan, S. K. Tetrahedron 1999, 55, 11331–11342.
[51] Shumilkina, E. A.; Borschev, O. V.; Ponomarenko, S. A.; Surin, N. M.; Pleshkova, A. P.; Muzafarov, A. M. Mendeleev Commun 2007, 17, 34–36.
[52] Schaefer, A.; Horn, H.; Ahlrichs, R. J. Chem Phys 1992, 97, 2571–2577.
[53] Granovsky, A. A., Firefly version 8.0.0. Available at http://classic.chem.msu.su/gran/firefly/firefly8_rc.html.
[54] Schmidt, M. W.; Baldridge, K. K.; Boatz, J. A.; Elbert, S. T.; Gordon, M. S.; Jensen, J. H.; Koseki, S.; Matsunaga, N.; Nguyen, K. A.; Su, S.; Windus, T. L.; Dupuis, M.; Montgomery, J. A. J Comput Chem 1993, 14, 1347–1363.